2020

MHD heat transfer in W-shaped inclined cavity containing a porous medium saturated with Ag/Al2O3 hybrid nanofluid in the presence of uniform heat generation/absorption

Mohamed Dhia Massoudi

Mohamed Bechir Ben Hamida

Hussein A. Mohammed
Edith Cowan University

Mohammed A. Almeshaal

10.3390/en13133457

Dhia Massoudi, M., Ben Hamida, M. B., Mohammed, H. A., & Almeshaal, M. A. (2020). MHD heat transfer in W-shaped inclined cavity containing a porous medium saturated with Ag/Al2O3 hybrid nanofluid in the presence of uniform heat generation/absorption. *Energies, 13*(13), 3457. https://doi.org/10.3390/en13133457

energies

MDPI

Article

MHD Heat Transfer in W-Shaped Inclined Cavity Containing a Porous Medium Saturated with Ag/Al_2O_3 Hybrid Nanofluid in the Presence of Uniform Heat Generation/Absorption

Mohamed Dhia Massoudi [1], Mohamed Bechir Ben Hamida [1,2,3,*], Hussein A. Mohammed [4,*] and Mohammed A. Almeshaal [5]

1 Research Unit of Ionized Backgrounds and Reagents Studies, Preparatory Institute for Engineering Studies of Monastir (IPEIM), University of Monastir, Monastir 5019, Tunisia; Meddhia1993@gmail.com
2 Chemical Engineering Department, College of Engineering, Ha'il University, Hail City 2240, Saudi Arabia
3 Physics Department, Higher School of Sciences and Technology of Hammam Sousse (ESSTHS), 4011 Lamine Abassi Street, University of Sousse, Sousse 4011, Tunisia
4 School of Engineering, Edith Cowan University, 270 Joondalup Drive, Joondalup, WA 6027, Australia
5 Department of Mechanical Engineering, College of Engineering, Al Imam Mohammad Ibn Saud Islamic University, Riyadh 11432, Saudi Arabia; maalmeshaal@imamu.edu.sa
* Correspondence: Mo.Benhamida@uoh.edu.sa or benhamida_mbechir@yahoo.fr (M.B.B.H.); Hussein.mohammed@ecu.edu.au or Hussein.dash@yahoo.com (H.A.M.)

Received: 23 March 2020; Accepted: 18 June 2020; Published: 3 July 2020

Abstract: In this paper, a 2D numerical study of natural convection heat transfer in a W-shaped inclined enclosure with a variable aspect ratio was performed. The enclosure contained a porous medium saturated with Ag/Al_2O_3 hybrid nanofluid in the presence of uniform heat generation or absorption under the effect of a uniform magnetic field. The vertical walls of the enclosure were heated differentially; however, the top and bottom walls were kept insulated. The governing equations were solved with numerical simulation software COMSOL Multiphysics which is based on the finite element method. The results showed that the convection heat transfer was improved with the increase of the aspect ratio; the average Nusselt number reached a maximum for an aspect ratio (AR) = 0.7 and the effect of the inclination was practically negligible for an aspect ratio of AR = 0.7. The maximum heat transfer performance was obtained for an inclination of $\omega = 15$ and the minimum is obtained for $\omega = 30$. The addition of composite nanoparticles ameliorated the convection heat transfer performance. This effect was proportional to the increase of Rayleigh and Darcy numbers, the aspect ratio and the fraction of Ag in the volumetric fraction of nanoparticles.

Keywords: free convection; W-shaped inclined enclosure; porous medium; hybrid nanofluid; uniform heat generation or absorption

1. Introduction

Magneto hydrodynamic (MHD) heat transfer has attracted a great deal of attention in the last few years, and it has been the subject of a vast number of research articles. This is because of the importance of this topic in different engineering applications for different domains such as crystal formation, geothermal energy and nuclear energy.

The enhancement of heat transfer has been the objective of many research articles in different applications such as discharge lamps [1–11]. In the same research area, many studies have been established to examine the natural convection heat transfer inside a porous medium due to the

importance of this scientific research in many engineering applications, such as in solar collectors, the cooling of micro-electromechanical systems (MEMS) and various industrial applications, as reported by Pop and Ingham [12], Bejan et al. [13], Vafai [14], Sankar et al. [15] and Ben Hamida et al. [16]. Chamkha and Selimefendigil [17] examined the generation of entropy and the natural convection inside a square corrugated cavity filled with porous medium saturated with nanofluid under the magnetic field effect. The results showed that the increase of Grashof and Darcy numbers enhanced the convection heat transfer. Shao et al. [18] made a comparison between their own results obtained with the Fourier–Galerkin spectral method for the Darcy–Brinkman model and other results obtained with the developed finite element model. Importantly, they found a high degree of similarity of the results from the two methods.

Nanofluids are used to ameliorate the heat performance of heat exchangers, as reported in different works such as Mohammed et al. [19,20]; in refrigeration systems, based on the absorption phenomenon on automotive air-conditioning, as reported by Ramanathan et al. [21]; for falling film bubble absorption processes in vertical plates on refrigerating systems by using copper nanofluid, as reported by Ben Hamida et al. [22,23] and Ben Jaballah et al. [24]; and the effect of operating conditions such as those reported by Benhmidene et al. [25]. The results have shown an enhancement of the effective absorption ratio with the addition of copper solution nanofluid and that the heat flux depends on the tube diameter. In addition, Abdollahi et al. [26] studied the case of an interrupted microchannel heat sink with elliptical and diamond ribs using Al_2O_3/water nanofluid with different volume fractions. They showed that the ellipse ribs result in better performance for the microchannel than diamond ribs and no ribs.

Some works, such as that by Sheikholeslami et al. [27], have investigated the effect of the heat source length on the heat transfer performance of a nanofluid inside a cavity under a magnetic field. They found that the average Nusselt number was ameliorated by the augmentation of the heat source length; however, it was reduced by the increase of the Hartmann number.

Recently, several researchers have examined the magneto hydrodynamic heat transfer inside a cavity with different shapes. Yuan Ma et al. [28] and Hosseinizadeh and Sourtiji [29] successively numerically studied the convection heat transfer inside a U-shaped and L-shaped cavity filled with nanofluid. The results obtained show that the heat transfer performance was improved with the addition of nanoparticles and with the augmentation of the aspect ratio of cavity. Other studies, such as that by Abedini et al. [30], investigated the magneto hydrodynamic heat transfer performance inside a C-shaped baffled enclosure filled with nanofluid. The results showed that the increase of the aspect ratio and the introduction of baffles improved the heat transfer performance, and the maximum heat transfer was obtained for an aspect ratio of AR = 0.7 and a baffle length of B_f = 0.2. Another study performed by Hussein et al. [31] examined the magnetohydrodynamic heat transfer inside a T-shaped enclosure. They found that the promotion of the aspect ratio improved the circulation of dynamic flow and the Nusselt number; by contrast, an increase of the Hartmann number reduces these factors. In the same way, other studies, such as that by Armaghani et al. [32], investigated the effect of the addition of a baffle to the T-shaped enclosure. They discovered that the addition of a baffle significantly enhanced the heat transfer performance inside the cavity. The maximum performance was obtained for an aspect ratio of AR = 0.2 and a baffle length of B_f = 0.6. In some context, several works, such as those by Ahmed et al. [33], Hasan et al. [34] and Hussain et al. [35], studied the heat transfer inside a corrugated cavity containing porous media saturated with nanofluid under the magnetic field effect. This again highlights the importance of this geometry on the thermal designs of such systems. The results show that the corrugated shapes have a significant effect on the control of the convection inside cavities.

However, returning to the literature, no study has examined the magneto hydrodynamic heat transfer inside a W-shaped inclined enclosure which presents a portion of corrugated cavity with a porous medium saturated with hybrid nanofluid with variable aspect ratios. Therefore, the aim of this study was to perform a bi-dimensional numerical study of the natural convection in a W-shaped inclined enclosure. The W-shaped cavity with a variable aspect ratio (AR) contained a porous medium

saturated with Ag-Al_2O_3/ethylene glycol hybrid nanofluid in the presence of uniform heat generation or absorption (q^*). The enclosure was under the effect of horizontal and uniform magnetic fields. This study is performed using COMSOL Multiphysics commercial simulation software, based on the finite element method. Various parameters are examined in this study, such as Rayleigh, Hartmann and Darcy numbers, the aspect ratio, the angle of inclination ω, the solid volume of composite nanoparticles φ and the fraction of Ag in the volumetric fraction of nanoparticles (Fr) on the thermal and hydraulic characteristics.

2. Numerical Model

2.1. Simplifying Assumptions

In order to solve the governing equations, some simplifying assumptions are considered as follows:

- A thermal equilibrium is supposed between the water base fluid and the nanoparticles;
- The nanofluid is supposed to be Newtonian and incompressible;
- The flow is assumed to be steady and laminar;
- The radiation, the dissipation and Joule heating effects, the displacement currents and the induced magnetic field are neglected.

2.2. Boundary Conditions

The schematic diagram of the W-shaped inclined enclosure with a porous medium saturated with Ag-Al_2O_3/ethylene glycol hybrid nanofluid in the presence of uniform heat generation or absorption is shown in Figure 1. The temperature (T_h) is uniformly imposed along the vertical wall (1) and the temperature (T_c) is uniformly imposed along walls 2–5. The top and bottom walls—6 and 7—are kept insulated. The W-shaped inclined cavity is under the effect of a magnetic field with uniform strength B_0. The gravitational effect presents two components along the x and y-axes. The W-shaped cavity is inclined with an angle ω compared to the horizontal as shown in Figure 1.

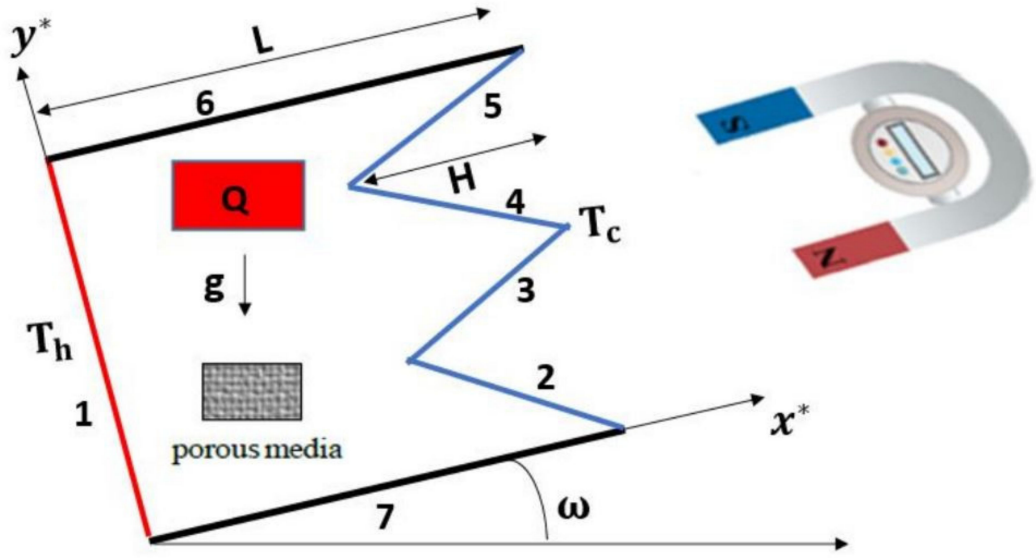

Figure 1. A schematic diagram of the physical model problem.

The boundary conditions used in a dimensionless form are presented in Table 1.

Table 1. The boundary conditions in dimensionless form.

Border	Condition On u*	Condition On v*	Condition On T*
1	0	0	1
2	0	0	0
3	0	0	0
4	0	0	0
5	0	0	0
6	0	0	$\frac{\partial T^*}{\partial y^*} = 0$
7	0	0	$\frac{\partial T^*}{\partial y^*} = 0$

2.3. Non-Dimensional Governing Equations

The Darcy law model was used to express the permeability of the porous medium. The following dimensionless parameter groups were proposed to express the dimensionless conservation equation system presented as follows:

$$x^* = \frac{x}{L},\ y^* = \frac{y}{L},\ u^* = \frac{u\,L}{\alpha_f},\ v^* = \frac{v\,L}{\alpha_f},\ T^* = \frac{T - T_c}{T_h - T_c},\ p^* = \frac{p\,L^2}{\rho_{hnf}\alpha_f^2},\ Pr = \frac{\vartheta_f}{\alpha_f},$$

$$Ha = B_0 L\sqrt{\frac{\sigma_{hnf}}{\rho_{hnf}\ \vartheta_f}},\ Ra = \frac{g\,\beta_f L^3(T_h - T_c)}{\vartheta_f \alpha_f},\ Da = \frac{K}{L^2},\ q^* = \frac{qL^2}{\alpha_{hnf}\left(\rho C_p\right)_{hnf}}$$

The mass conservation equation is as follows:

$$\frac{\partial u^*}{\partial x^*} + \frac{\partial v^*}{\partial y^*} = 0 \tag{1}$$

where u^* and v^* are the dimensionless velocities according to x^* and y^*, respectively.

The momentum conservation equation according to x^* is as follows:

$$u^*\frac{\partial u^*}{\partial x^*} + v^*\frac{\partial u^*}{\partial y^*} = -\frac{\partial p^*}{\partial x^*} + \mathrm{Pr}\frac{\alpha_{hnf}}{\alpha_f}\left(\frac{\partial^2 u^*}{\partial x^{*2}} + \frac{\partial^2 u^*}{\partial y^{*2}} - \frac{u^*}{Da}\right) + \frac{(\rho\beta)_{hnf}}{\rho_{hnf}\beta_f}RaPr\theta\ \sin(\omega) \tag{2}$$

where ρ_{hnf} and p^* are the density of the hybrid nanofluid and the dimensionless fluid pressure, respectively.

The momentum conservation equation according to y^* is as follows:

$$u^*\frac{\partial v^*}{\partial x^*} + v^*\frac{\partial v^*}{\partial y^*} = -\frac{\partial p^*}{\partial y^*} + Pr\frac{\alpha_{hnf}}{\alpha_f}\left(\frac{\partial^2 v^*}{\partial x^{*2}} + \frac{\partial^2 v^*}{\partial y^{*2}} - \frac{v^*}{Da}\right) + \frac{(\rho\beta)_{hnf}}{\rho_{hnf}\beta_f}RaPr\theta\ \cos(\omega) - Ha^2 Prv^* \tag{3}$$

where β is the thermal expansion coefficient of the hybrid nanofluid.

The energy conservation equation is as follows:

$$u^*\frac{\partial T^*}{\partial x^*} + v^*\frac{\partial T^*}{\partial y^*} = \frac{\alpha_{hnf}}{\alpha_f}\left(\frac{\partial^2 T^*}{\partial x^{*2}} + \frac{\partial^2 T^*}{\partial y^{*2}}\right) + \frac{\alpha_{hnf}T^*}{\alpha_f}q^* \tag{4}$$

where α_{nf} is the thermal diffusivity of the nanofluid.

The effective density and electrical conductivity of the hybrid nanofluid can be calculated using

$$\rho_{hnf} = (1-\varphi)\rho_f + \varphi_{Ag}\rho_{Ag} + \varphi_{Al_2O_3}\rho_{Al_2O_3} \tag{5}$$

$$\sigma_{hnf} = (1-\varphi)\sigma_f + \varphi_{Ag}\sigma_{Ag} + \varphi_{Al_2O_3}\sigma_{Al_2O_3} \tag{6}$$

where φ is the overall volume concentration of composite nanoparticles:

$$\varphi = \varphi_{Ag} + \varphi_{Al_2O_3}$$

Furthermore, the fraction of Ag in the volumetric fraction of nanoparticles is defined as

$$Fr = \frac{\varphi_{Ag}}{\varphi_{Ag} + \varphi_{Al_2O_3}} \tag{7}$$

The effective heat capacitance and coefficient of thermal dilatation of the nanofluid are given by [36]

$$\left(\rho C_p\right)_{hnf} = (1-\varphi)\left(\rho C_p\right)_f + \varphi_{Ag}\left(\rho C_p\right)_{Ag} + \varphi_{Al_2O_3}\left(\rho C_p\right)_{Al_2O_3} \tag{8}$$

$$(\rho\beta)_{hnf} = (1-\varphi)(\rho\beta)_f + \varphi_{Ag}(\rho\beta)_{Ag} + \varphi_{Al_2O_3}(\rho\beta)_{Al_2O_3} \tag{9}$$

$$\alpha_{hnf} = \frac{k_{hnf}}{\left(\rho C_p\right)_{hnf}} \tag{10}$$

Brinkman's [37] model is used for the effective dynamic viscosity of the hybrid nanofluid:

$$\mu_{hnf} = \frac{\mu_f}{\left(1-(\varphi_{Ag} + \varphi_{Al_2O_3})\right)^{2.5}} \tag{11}$$

The effective thermal conductivity of the hybrid nanofluid is given by Maxwell [38]:

$$\frac{k_{hnf}}{knf} = \frac{\frac{1}{\varphi}(\varphi_{Ag}k_{Ag} + \varphi_{Al_2O_3}k_{Al_2O_3}) + 2k_f + 2(\varphi_{Ag}k_{Ag} + \varphi_{Al_2O_3}k_{Al_2O_3}) - 2\varphi k_f}{\frac{1}{\varphi}(\varphi_{Ag}k_{Ag} + \varphi_{Al_2O_3}k_{Al_2O_3}) + 2k_f \ -(\varphi_{Ag}k_{Ag} + \varphi_{Al_2O_3}k_{Al_2O_3}) + \varphi k_f} \tag{12}$$

The thermophysical properties of the base fluid (ethylene glycol) with Ag and Al_2O_3 [39] are given in Table 2.

Table 2. The thermophysical properties of the base fluid (ethylene glycol) with Ag and Al_2O_3 nanoparticles.

Basic Fluid and Nanoparticles	Pr	ρ (kg/m^3)	Cp (J/kg·K)	k (W/m·K)	$\beta \times 10^{-5}$ (K^{-1})	μ (Kg/ms)
Ethylene Glycol	151	1109	2400	0.26	65	0.0163
Al_2O_3		3970	765	40	0.85	-
Ag		10,500	535.6	429	0.85	-

The governing equations are solved by using the commercial simulation software COMSOL Multiphysics, which is based on the finite element technique.

2.4. Nusselt Number Calculation

The local Nusselt number on the left hot wall can be formalized as

$$Nu_l = -\frac{k_{nf}}{k_f}\left(\frac{\partial T^*}{\partial x^*}\right)_{x^*=0} \tag{13}$$

The average Nusselt number (Nu_m) is calculated by integrating Nu_{x^*} along the hot wall:

$$Nu_m = \int_0^1 -\frac{k_{nf}}{k_f}\left(\frac{\partial T^*}{\partial x^*}\right)_{x^*=0} \partial y^* \tag{14}$$

2.5. Solution Procedure and Grid Sensitivity Test

The system of governing equations is solved considering the boundary conditions by using the commercial simulation software COMSOL Multiphysics, which is based on the finite element technique.

Figure 2 shows the triangular mesh distribution along the enclosure. The sensitivity of several grids for choosing a sufficient predefined mesh size for which the results are independent is presented in Table 3. As indicated in Table 3, a finer mesh was chosen for the numerical estimation taking into account the exactness and the calculation time.

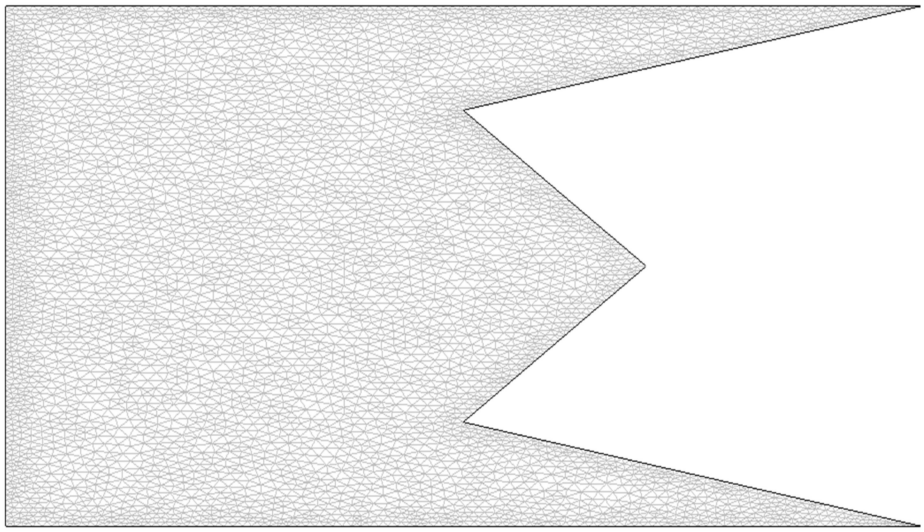

Figure 2. A schematic of the mesh distribution.

Table 3. Grid sensitivity check for Ra $= 10^5$, Ha $= 0$, $\varphi = 0.04$, $q^* = 1$, Da $= 10^{-2}$ and $\omega = 0$. Ra: Rayleigh number; Ha: Hartmann number; Da: Darcy number; φ: solid volume of composite nanoparticles; ω : angle of inclination.

Predefined Mesh Size	Mesh Elements	Nu_m	CPU Time (s)
Extremely coarse	1846	4.6897	4.63
Extra coarse	2210	4.6924	5.589
Coarser	3092	4.6976	7.56
Coarse	3654	4.6974	9.072
Normal	4608	4.6980	11.475
Fine	4710	4.6980	12.796
Finer	5784	4.6984	14.901
Extra fine	9182	4.6980	20.765
Extremely fine	28,368	4.6981	108.848

3. Results and Discussion

The numerical simulations were conducted under the condition of natural convection heat transfer in a W-shaped inclined enclosure with a porous medium saturated with hybrid nanofluid, with variable aspect ratios and with the presence of uniform heat generation or absorption. Various parameters are examined in this study, such as Rayleigh, Hartmann and Darcy numbers, the aspect ratio, the angle of inclination ω, the solid volume of composites nanoparticles φ and the fraction of Ag in the volumetric fraction of nanoparticles (Fr) on the thermal and hydraulic characteristics. The effects of these parameters on the thermal and hydraulic characteristics are interpreted and presented in this section.

3.1. Validation

In order to validate the present results, a comparison was performed between the present results obtained with the results from a 2D study by Chamkha and Selimefendigil [17]. The streamlines and isotherms for different values of Da $= 10^{-4}, 10^{-3}$ and 10^{-1} for Gr $= 10^4$, Ha $= 10$ and $\varphi = 0.02$ were compared. As shown in Figures 3 and 4, a good agreement was found between the two results. In addition, the average Nusselt number at the hot wall for Gr $= 510^4$, Da $= 10^{-2}$ and $\varphi = 0.02$ was compared with the results obtained by Chamkha and Selimefendigil [17]. The numerical domain was divided into 51×51 uniform spatially grids, and the same grids were adopted for this study. Table 4 shows an acceptable agreement between the present results and the results obtained by Chamkha and Selimefendigil [17].

Table 4. Validation of numerical code.

Ha	Nu_m Present Work	Nu_m Chamkha and Selimefendigil [17]
0	7.4103	7.4019
10	7.1514	7.1315
20	6.5125	6.5059
30	5.8725	5.8709
40	5.17	5.1612
50	4.5505	4.5483

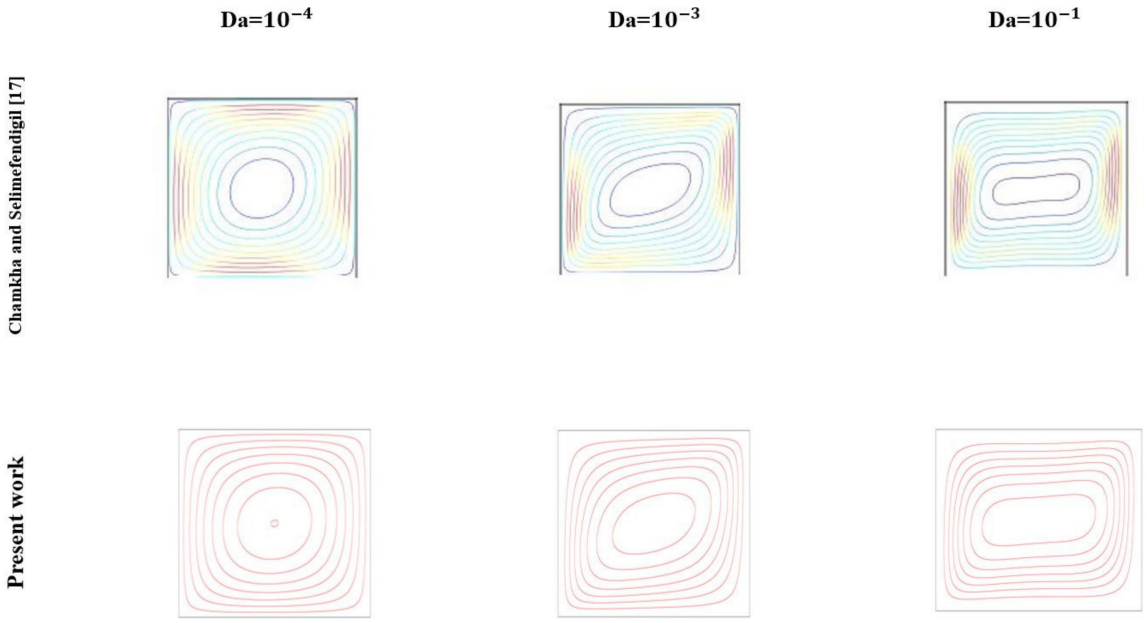

Figure 3. Streamlines for different Darcy numbers with Grashof number $Gr = 10^4$, Ha = 10 and $\varphi = 0.02$.

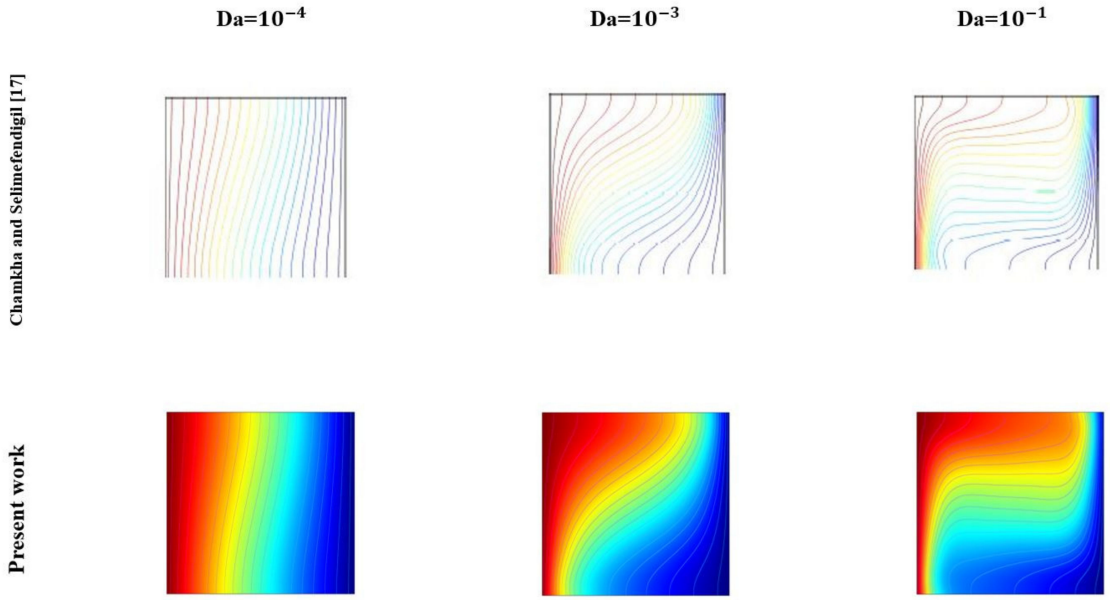

Figure 4. Isotherms for different Darcy numbers with Grashof number $Gr = 10^4$, Ha = 10 and $\varphi = 0.02$.

The analysis is performed for a constant Prandtl number value of 151 and the effects of the Rayleigh number (Ra), Hartmann number (Ha), the Darcy number (Da), the aspect ratio (AR), the angle of inclination (ω), the solid volume of composite nanoparticles (φ) and the fraction of Ag in the volumetric fraction of nanoparticles (Fr) on the distribution of the isotherms, the streamlines, the average Nusselt number and the heat transfer performance inside the cavity are presented and discussed in the following sections.

3.2. Effect of Rayleigh and Hartmann Numbers

In this section, the effect of Rayleigh and Hartmann numbers on the isotherms, streamlines and heat transfer performance is examined. The aspect ratio AR = 0.3, $\omega = 0$, Fr = 0.75, Da $= 10^{-2}$ and $q^* = 1$ are kept constant.

Figures 5 and 6 present the distribution of the isotherms and streamlines between the hot and cold walls for different values of Rayleigh and Hartmann numbers; respectively, Ra $= 10^3$, 10^4, 10^5 and 10^6 and Ha = 0, 15, 30 and 45 for a constant of $\varphi = 0.04$. The results exhibited in Figures 5 and 6 show that, for a low Rayleigh number, the flow behavior takes a circular shape with a deformation of the circular shape near the cold wall. The augmentation of the Rayleigh number leads to a deformation of the circular flow shape, which is stretched in form, especially near the cold wall, for higher Rayleigh numbers. In addition, it can be observed that that the increase of the Rayleigh number intensifies the flow velocity of the hybrid nanofluid, which is because of the augmentation of the effect of buoyancy force inside the cavity, especially near the walls. Therefore, it is observed that the promotion of the convective heat transfer compared to the conductivity inside the cavity between the hybrid nanofluid and the hot wall is more pronounced. In the same context, the effect of the buoyancy force inside the cavity by the increase of the Rayleigh number is made more pronounced by the change in the distribution of the isotherms. For a low Rayleigh number, where a conductive regime is predominant, the isotherms between the cold and hot walls are parallel; then, they become horizontal between the top and bottom walls for a higher Rayleigh number where the convection is predominant. Therefore, the results show that the augmentation of the Rayleigh number enhances the convection heat transfer inside the cavity due to the augmentation of the effect of the buoyancy force. To better examine the effect of the Rayleigh number on the heat transfer rate, the variation of the average Nusselt number at the hot wall for different values of Rayleigh numbers is shown in Figure 7. As illustrated in Figure 7, it can clearly be seen that the increase of the Rayleigh number leads to the promotion of the average

Nusselt number at the level of the hot wall, which means that the enhancement of the convection heat transfer between the hybrid nanofluid and the hot wall is more significant. The increase of the average Nusselt number Nu_m with the augmentation of the solid fraction of composite nanoparticles φ can also be observed, as shown in Figure 7.

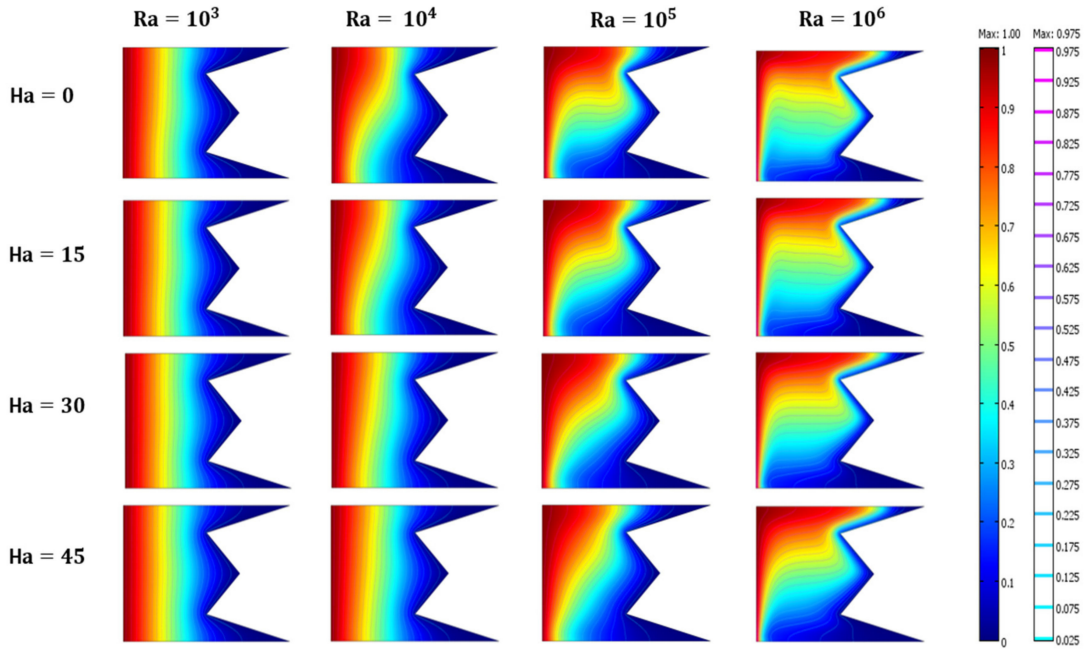

Figure 5. Isotherms for different values of Rayleigh numbers (Ra $= 10^3$, 10^4, 10^5 and 10^6) and Hartmann numbers (Ha = 0, 15, 30 and 45), Da $= 10^{-2}$, aspect ratio (AR) = 0.3, $\omega = 0$, $\varphi = 0.04$, Fr = 0.75 and $q^* = 1$.

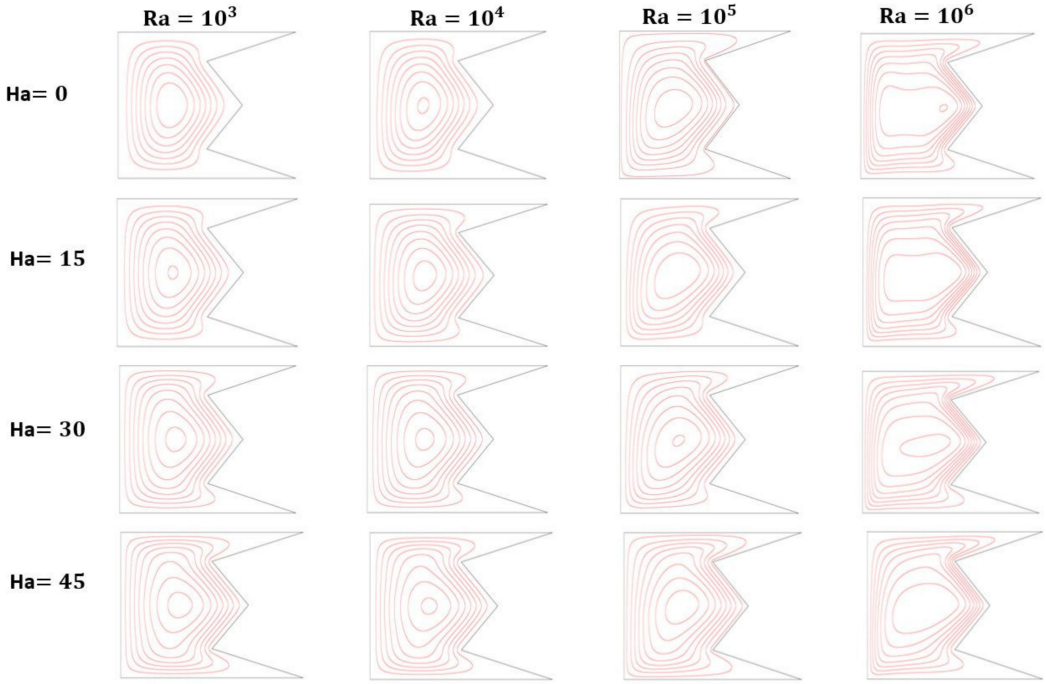

Figure 6. Streamlines for different values of Rayleigh numbers (Ra $= 10^3$, 10^4, 10^5 and 10^6) and Hartmann numbers (Ha = 0, 15, 30 and 45), Da $= 10^{-2}$, AR = 0.3, $\omega = 0$, $\varphi = 0.04$, Fr = 0.75 and $q^* = 1$.

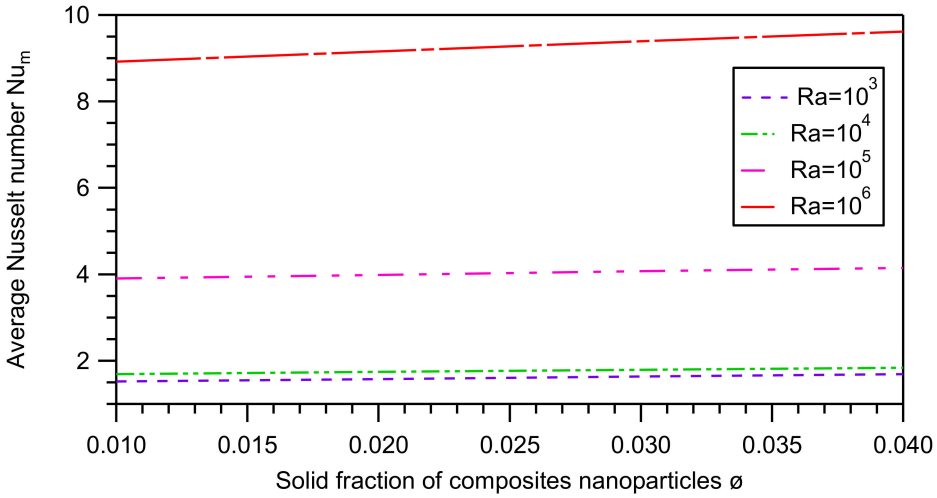

Figure 7. The average Nusselt number Nu_m according to the solid fraction of composite nanoparticles φ for different values of Rayleigh numbers (Ra $= 10^3$, 10^4, 10^5 and 10^6) with Ha = 15, Da $= 10^{-2}$, AR = 0.3, $\omega = 0$, Fr = 0.75 and $q^* = 1$.

According to Figures 5 and 6, it can be observed that the space between the streamlines is reduced, particularly near the top and bottom walls. Moreover, a deformation represented as a vertical prolongation of the circular shape of the streamlines can be observed with a reduction in the intensification of the flow velocity field near the walls. This can be explained by the effect of the Lorentz forces created by the magnetic field; these forces surmount the effect of the buoyancy force and hinder the flow rate. Looking at the isotherms, the distortion of the horizontal lines of isotherms can obviously be seen between the top and bottom walls in proportion to the augmentation of the Hartmann number. Consequently, the demotion of the convection heat transfer inside the cavity with the increase of the Hartmann number and the transition from a dominant convection to conduction regime is observed.

Figure 8 presents the evolution of the average Nusselt number according to the Hartmann number for different Rayleigh numbers (Ra $= 10^3$, 10^4, $10^5$and 10^6). It can be seen that that the maximum average Nusselt number is obtained for Ha = 0, which shows the absence of a magnetic field effect. Thus, the diminution of the average Nusselt number is proportional and related to the increase of the effect of the Lorentz forces induced by the application of the magnetic field, especially for a medium convection flux inside the cavity for Ra $= 10^5$.

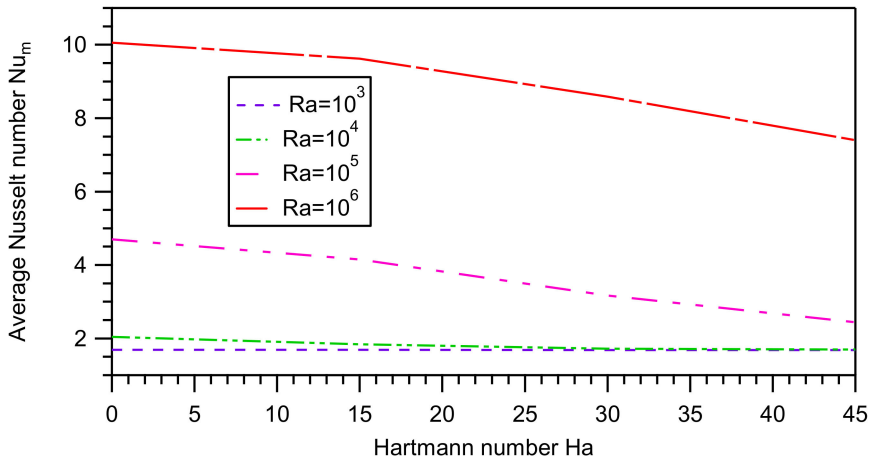

Figure 8. The average Nusselt number Nu_m for different values of Rayleigh number (Ra $= 10^3$, 10^4, 10^5 and 10^6) with Da $= 10^{-2}$, AR = 0.3, $\omega = 0$, $\varphi = 0.04$, Fr = 0.75 and $q^* = 1$.

3.3. *Effect of Darcy Number*

In this section, the effect of the Darcy number on the isotherms, the streamlines and the convection heat transfer performance is investigated. The Hartmann number is kept constant at Ha = 15, AR = 0.3, $\omega = 0$, Fr = 0.75 and $q^* = 1$.

Figures 9 and 10 present the isotherms and streamlines and for different Darcy and Rayleigh numbers for a Hartmann number of Ha = 15. It can be seen that for a low Darcy number and low permeability of porous medium, a conduction regime is predominant inside the cavity, and this is pronounced due to the vertical repartition of the isotherms between the heated walls. The increase of the Darcy number leads to the amelioration of the convection heat transfer between walls. Figure 11 shows the average Nusselt number according to the Darcy number for different Rayleigh number values. It can be observed that the increase of the Darcy number does not present a significant effect on the variation of the average Nusselt number for a low Rayleigh number when the conduction regime is predominant. In contrast, for a medium and higher Rayleigh number when medium and strong convection inside the cavity is predominant, it can be observed that the increase of the Darcy number leads to the promotion of the average Nusselt number, and consequently, the convection heat transfer is ameliorated in proportion to the increase of the permeability of the porous medium.

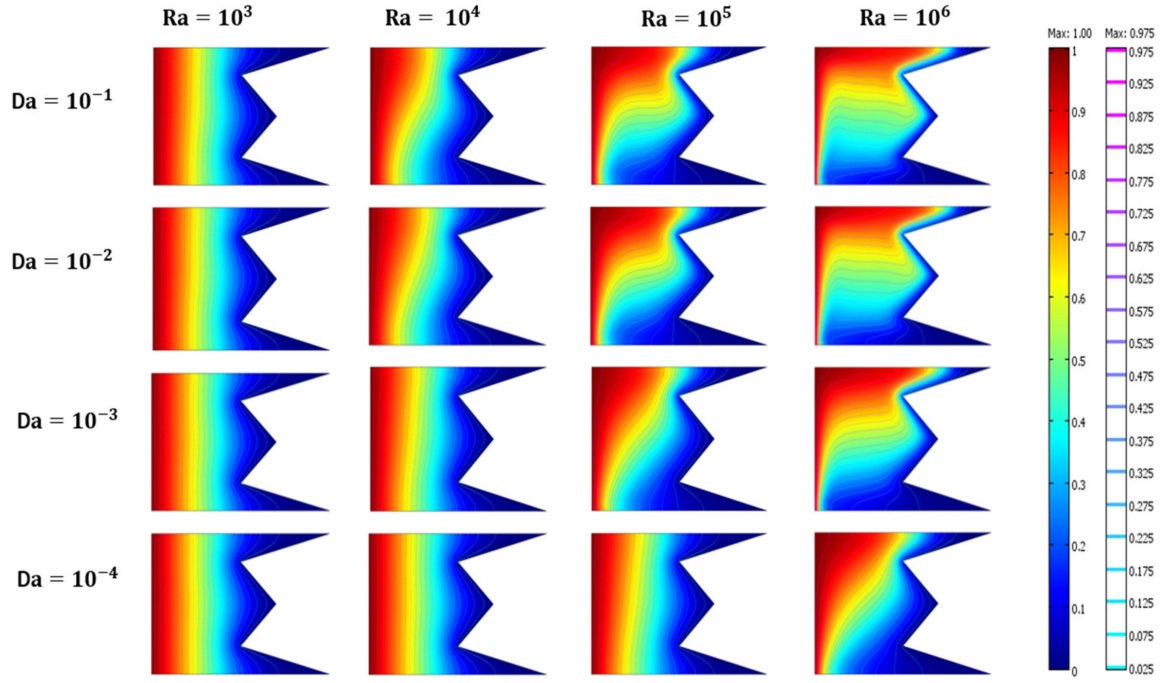

Figure 9. Isotherms for different values of Darcy numbers (Da $= 10^{-4}$, 10^{-3}, 10^{-2} and 10^{-1}) and Rayleigh numbers (Ra $= 10^3$, 10^4, 10^5 and 10^6), Ha = 15, AR = 0.3, $\omega = 0$, $\varphi = 0.04$, Fr = 0.75 and $q^* = 1$.

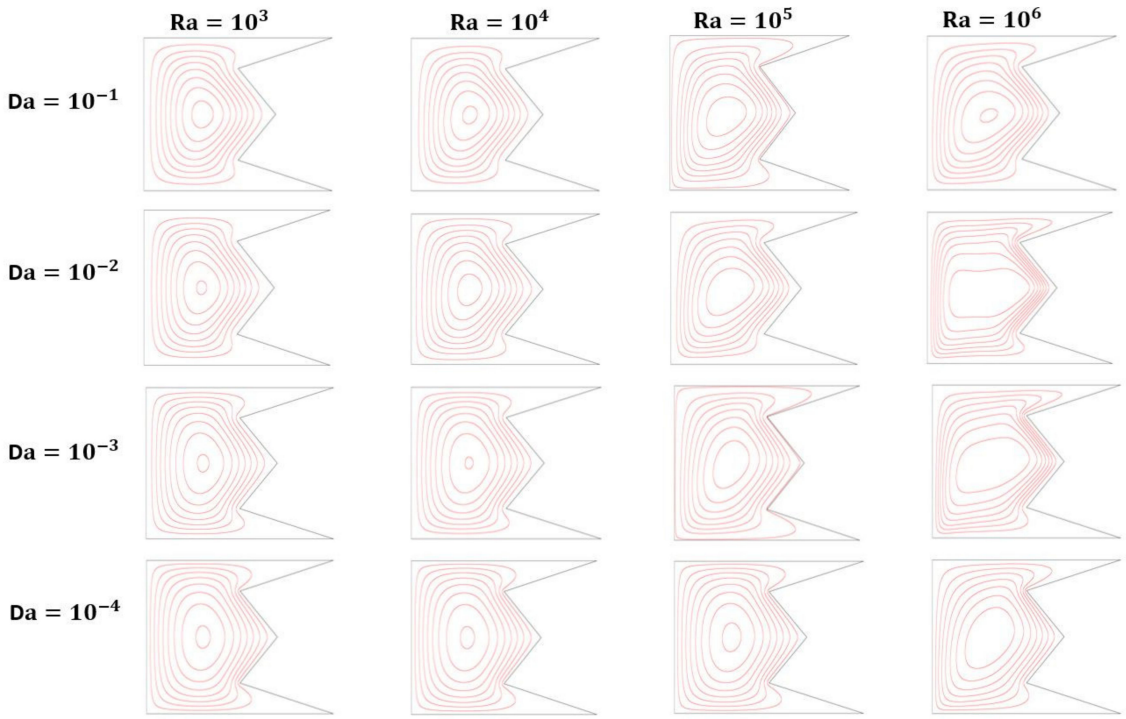

Figure 10. The streamlines for different values of Darcy numbers (Da $= 10^{-4}$, 10^{-3}, 10^{-2} and 10^{-1}) and Rayleigh numbers (Ra $= 10^3$, 10^4, 10^5 and 10^6), Ha = 15, AR = 0.3, $\omega = 0$, $\varphi = 0.04$, Fr = 0.75 and $q^* = 1$.

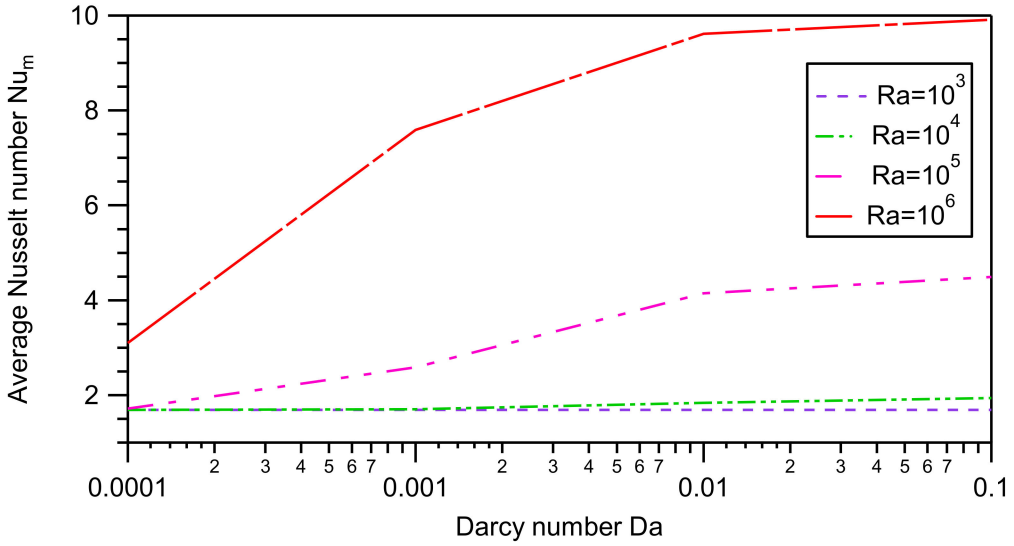

Figure 11. The average Nusselt number Nu_m according to the Darcy number Da for different values of Rayleigh number (Ra $= 10^3$, 10^4, 10^5 and 10^6) with AR = 0.3, $\omega = 0$, $\varphi = 0.04$, Fr = 0.75 and $q^* = 1$.

Figure 12 presents the average Nusselt number according to the solid fraction of the composite nanoparticles for different ranges of Darcy numbers. It can be clearly seen that the addition of composite nanoparticles increases the average Nusselt number. This effect is proportional to the increase of the Darcy number when the heat transfer regime changes from a conductive to a convective regime.

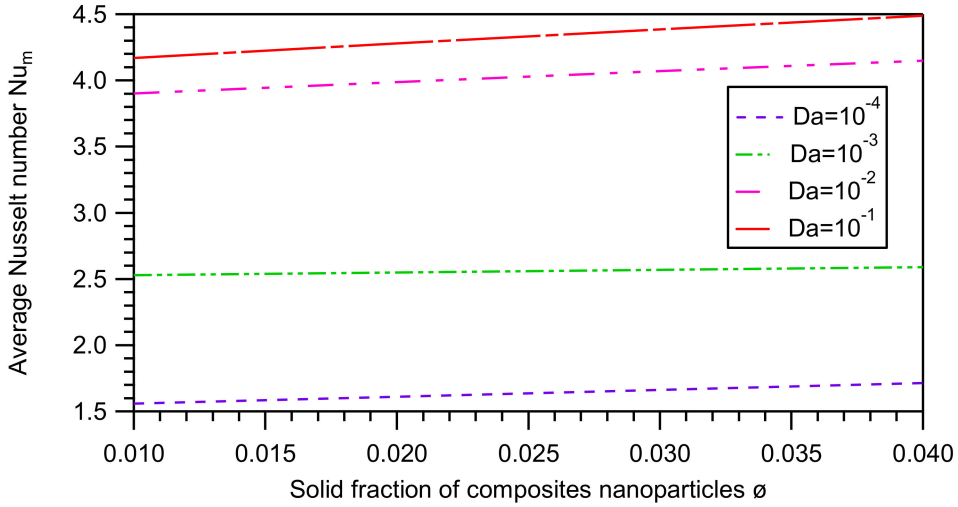

Figure 12. The average Nusselt number Nu_m according to solid fraction of composite nanoparticles φ for different values of Darcy number (Da $= 10^{-4}$, 10^{-3}, 10^{-2} and 10^{-1}) with Ra $= 10^5$, Ha = 15, AR = 0.3, $\omega = 0$ and $q^* = 1$.

3.4. Effect of the Aspect Ratio of the W-Shaped Enclosure

In this section, the effect of the aspect ratio on the isotherms, streamlines and the convection heat transfer performance is investigated. The Hartmann number is fixed at Ha = 15, $\omega = 0$, Fr = 0.75 and $q^* = 1$.

The results shown in Figure 13 present the streamlines for different aspect ratios and Rayleigh number values, revealing that the augmentation of the aspect ratio leads to a decrease in the volume of the vortices inside the cavity. Moreover, it can be seen that the circular form of the current lines undergoes a vertical dilation in terms of their shape, as well as a rapprochement occurring between the lines, due to the reduction in the circulation space of the fluid flow inside the cavity; this is proportional to the increase of the aspect ratio. In addition, it can be seen that the augmentation of the aspect ratio reduces the space for the fluid flow circulation near the heated walls.

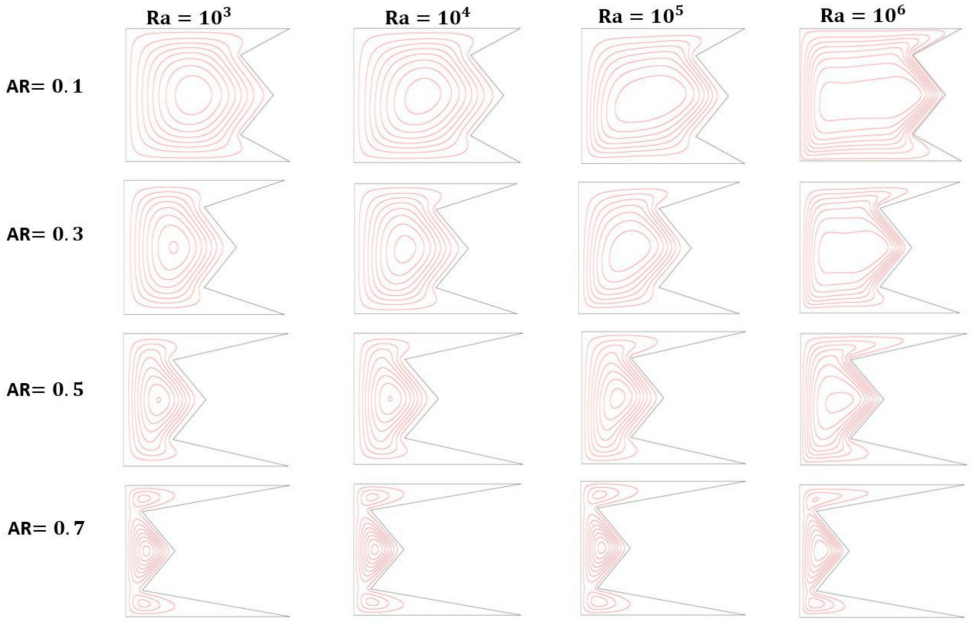

Figure 13. Streamlines for different values of aspect ratio (AR = 0.1, 0.3, 0.5 and 0.7) and Rayleigh number (Ra $= 10^3$, 10^4, 10^5 and 10^6) with Ha = 15, Da $= 10^{-2}$, $\omega = 0$ and $q^* = 1$.

It can also be noticed that, for the case of AR = 0.7, the creation of two vortices near the top and bottom left walls is more pronounced. Moreover, the streamlines become more intensified near the heated walls, meaning the increase of the velocity is proportional to the augmentation of buoyancy forces.

Figure 14 presents the isotherms for different aspect ratios and Rayleigh number values. According to Figure 14, the isotherms between the boundary heated walls become compressed as soon as the aspect ratio increases; this has the result of decreasing the flow of hybrid nanofluid between the heated walls, and consequently an improvement in heat transfer occurs.

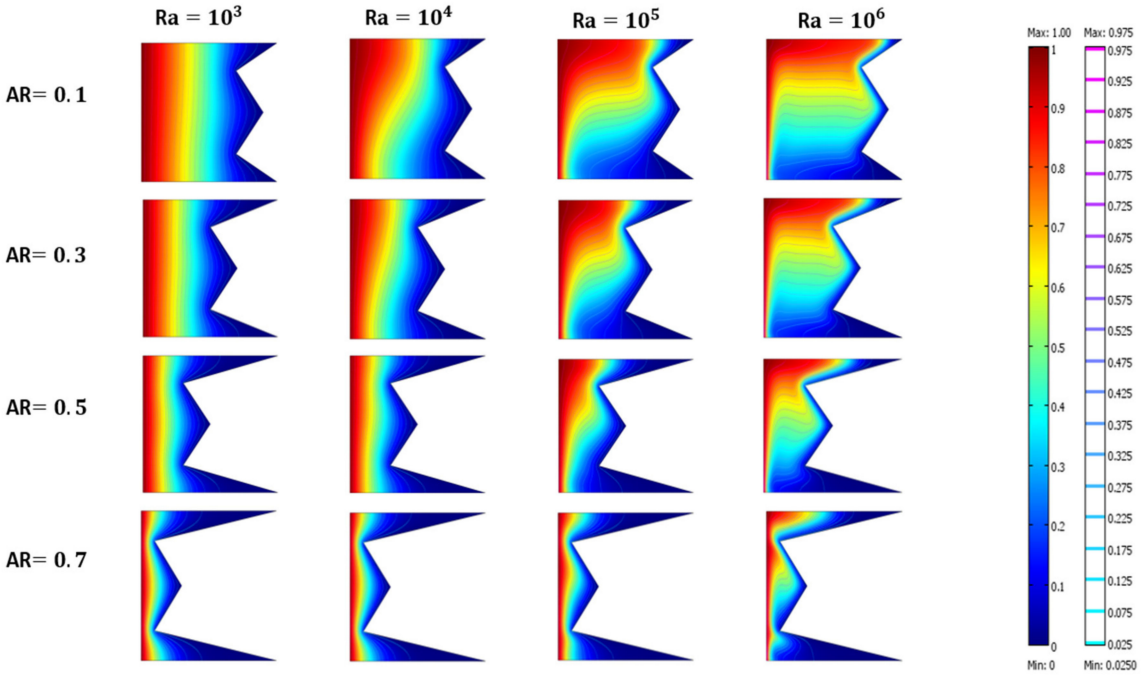

Figure 14. Isotherms for different values of aspect ratio (AR = 0.1, 0.3, 0.5 and 0.7) and Rayleigh number (Ra $= 10^3$, 10^4, 10^5 and 10^6) with Ha = 15, Da $= 10^{-2}$, $\omega = 0$ and $q^* = 1$.

Figure 15 shows the average Nusselt number for different aspect ratios and Darcy number values. This figure illustrates that the increase of the aspect ratio leads to the amelioration of the convection heat transfer inside the cavity. The maximum heat transfer is obtained for an aspect ratio of AR = 0.7. On the other hand, Figure 16 presents the average Nusselt according to the Hartmann number for different aspect ratios; the increase of the Hartmann number causes a decrease in the convection heat transfer. It can be seen that the effect of the magnetic field is minor for an aspect ratio of AR = 0.7 when the diminution of the average Nusselt number is slight. This is due to the predominance of the convection flow compared to the Lorentz forces.

3.5. Effect of the Inclination of the W-Shaped Cavity

In this section, the effect of the inclination of the W-shaped cavity on the isotherms, streamlines and the convection heat transfer performance is investigated. The Hartmann and Rayleigh numbers are fixed successively at Ha = 15, Ra $= 10^5$, Da $= 10^{-2}$ and $q^* = 1$.

The effect of the angle of inclination of the cavity on the isotherms, streamlines and the heat transfer performance for different aspect ratios—respectively, AR = 0.1, 0.3, 0.5 and 0.7—is shown in Figures 17 and 18. As shown in Figures 17 and 18, for AR = 0.3, the deformation of the streamlines and the isotherms between the heated walls can be observed with the variation of the inclination of the cavity, especially for the two case where s $\omega = 15$; it is clear that the cold isotherms move closer to the top hot wall and an enhancement of convection heat transfer is obtained, which indicates an increasing effect of the buoyancy forces compared to the Lorentz forces. However, for $\omega = 30$, the distortion of the isotherms and a change from convective to conductive regime inside the cavity can be clearly observed. On the other hand, for AR = 0.7, it can be seen that the variation of the inclination of the cavity does not have an important effect on the isotherms and the streamlines between the boundary heated walls, with the exception of $\omega = 30$, for which the location of the flow is concentrated on the bottom wall.

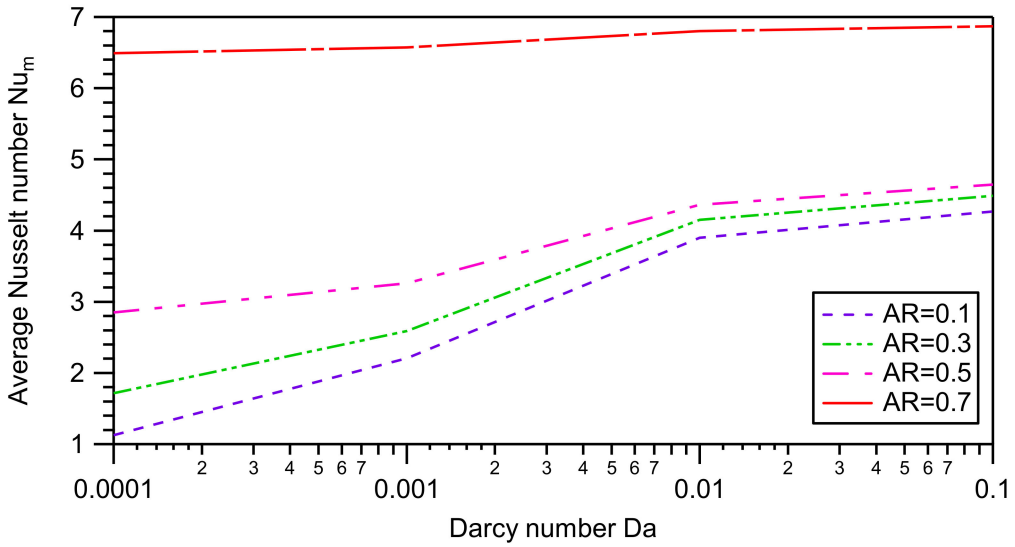

Figure 15. The average Nusselt number Nu_m according to the Darcy number with different aspect ratios (AR = 0.1, 0.3, 0.5 and 0.7) with Ra $= 10^5$, Ha = 15, $\varphi = 0.04$, Fr = 0.75, $\omega = 0$ and $q^* = 1$.

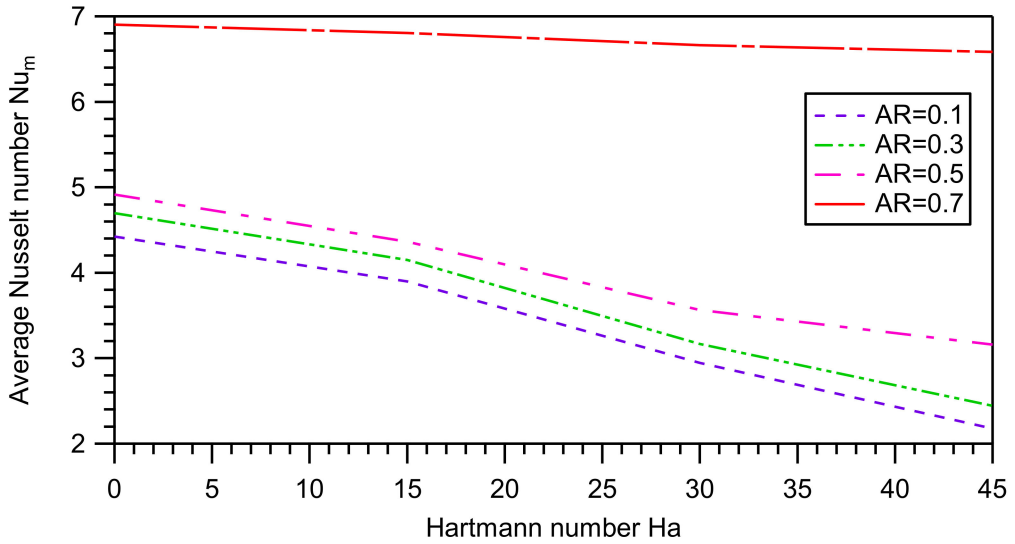

Figure 16. The average Nusselt number Nu_m according to the Hartmann number for different aspect ratios (AR = 0.1, 0.3, 0.5 and 0.7) with Ra $= 10^5$, Da $= 10^{-2}$, $\varphi = 0.04$, Fr = 0.75, $\omega = 0$ and $q^* = 1$.

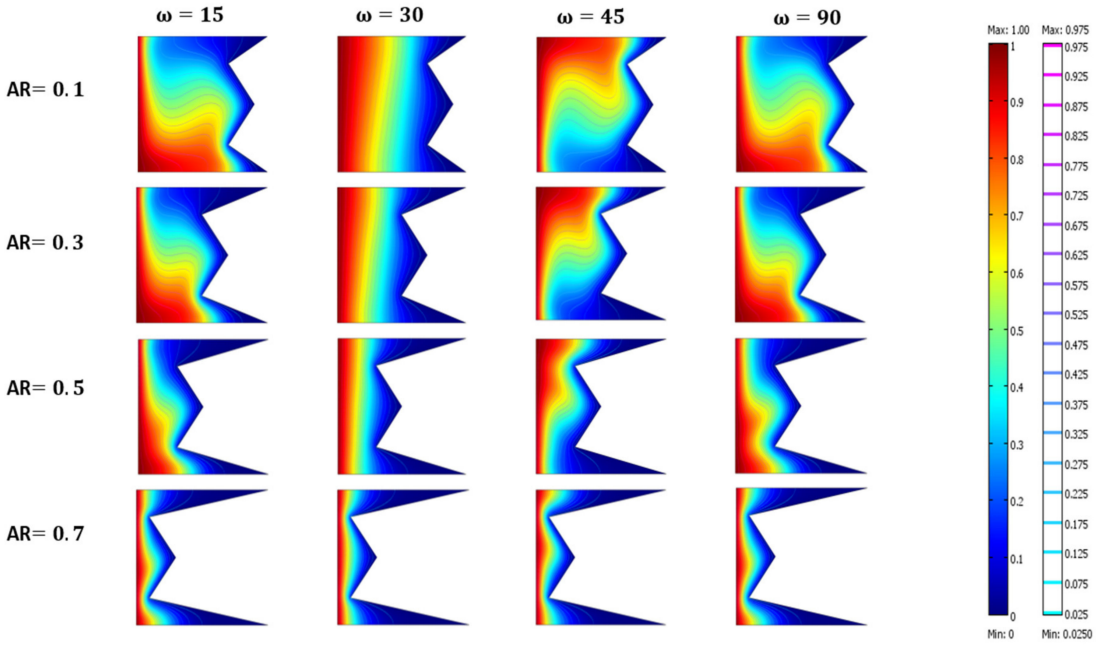

Figure 17. Isotherms for different angles of inclination ω and aspect ratios with Ra $= 10^5$, Ha = 15, Da $= 10^{-2}$, $\varphi = 0.04$, Fr = 0.75 and $q^* = 1$.

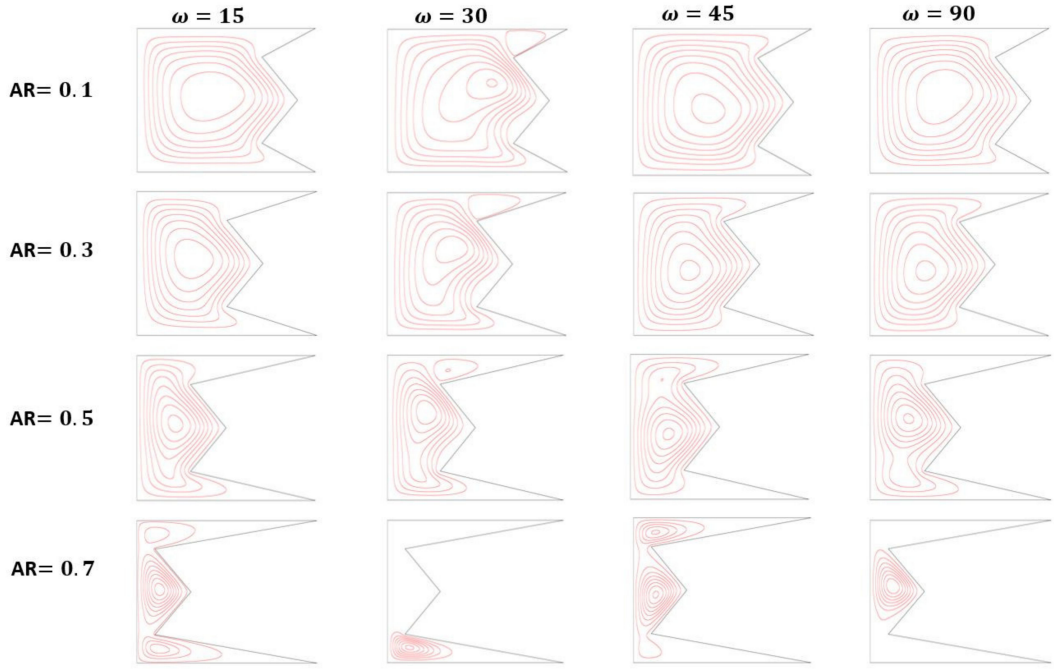

Figure 18. Streamlines for different angles of inclination ω and aspect ratios with Ra $= 10^5$, Ha = 15, Da $= 10^{-2}$, $\varphi = 0.04$, Fr = 0.75 and $q^* = 1$.

Figure 19 presents the average Nusselt number according to the angle of inclination for different aspect ratios. It can be seen that the convection heat transfer reaches a maximum value for $\omega = 15$ and a minimum value for $\omega = 30$.

In addition, it can be seen that the effect of the inclination of the cavity has a minor effect on the variation of the average Nusselt number for the case of AR = 0.7, for which the convection is dominant inside the cavity. Thus, the effect of the Lorentz and the buoyancy forces on the convection heat transfer is related to the value of angle of inclination of the cavity.

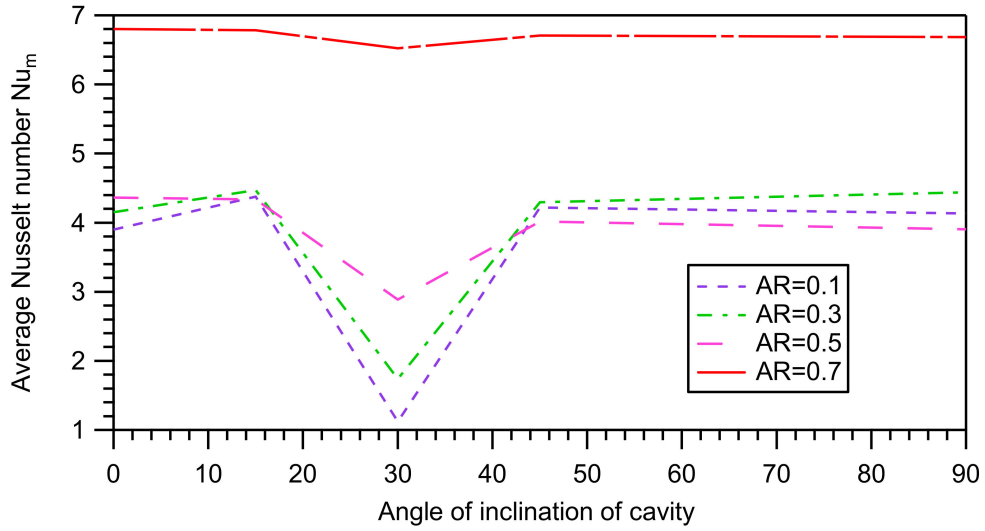

Figure 19. The average Nusselt number Nu_m according to the angle of inclination of the cavity for different aspect ratios (AR = 0.1, 0.3, 0.5 and 0.7) with Ra $= 10^5$, Da $= 10^{-2}$, $\varphi = 0.04$, Fr = 0.75, and $q^* = 1$.

3.6. Effect of the Fraction of Ag in the Volumetric Fraction of Nanoparticles

In this section, the effect of the fraction of Ag in the volumetric fraction of nanoparticles (Fr) on the convection heat transfer rate is investigated. The Hartmann, Rayleigh and Darcy numbers are fixed at Ha = 15, Ra $= 10^5$, Da $= 10^{-2}$, AR = 0.3, $\omega = 0$ and $q^* = 1$.

Based on the results obtained in Figures 7 and 12, and as shown in Figure 20, it can be noted that the increase of the solid volume of composite nanoparticles leads to the promotion of the average Nusselt number; consequently, the convection heat transfer rate is enhanced between the hybrid nanofluid and the hot wall. In addition, the augmentation of the average Nusselt number is proportional to the fraction of Ag in the volumetric fraction of nanoparticles (Fr); the more the fraction of Ag (Fr) is increased, the more the average Nusselt number is ameliorated.

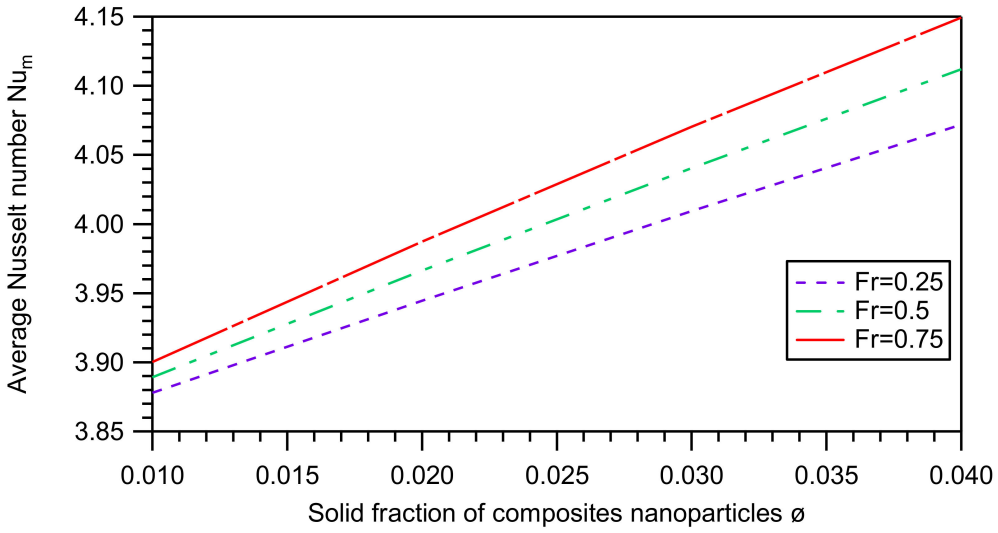

Figure 20. The average Nusselt number Nu_m for different fractional values of Ag in the volumetric fraction of nanoparticles (Fr = 0.25, 0.5 and 0.75) with Ra $=10^5$, Ha = 15, Da = 10^{-2}, AR = 0.3, and $q^* = 1$.

4. Conclusions

The MHD heat transfer inside a W-shaped inclined cavity filled with a porous medium saturated with Ag/Al_2O_3 hybrid nanofluid in the presence of uniform heat generation or absorption with a variable aspect ratio was studied in this work. The effects of the Rayleigh, Hartmann and Darcy numbers, the aspect ratio, the angle of inclination, the solid fraction of composites nanoparticles and the fraction of Ag in the volumetric fraction of nanoparticles were investigated.

The main conclusions obtained are as follows:

- The increase of the Rayleigh and Darcy numbers leads to the intensification of the hydrodynamic flow near the boundary heated walls and improves the convection heat transfer performance inside the cavity.
- The increase of the Hartmann number attenuates the convection heat transfer inside the cavity; this effect is insignificant for the case of an aspect ratio of AR = 0.7.
- The augmentation of the aspect ratio intensifies the hydrodynamic field and ameliorates the heat convection heat transfer performance. The convection heat transfer reaches a maximum for AR = 0.7.
- The average Nusselt number reaches its maximum for an angle of inclination $\omega = 15$ and a minimum for $\omega = 30$; the effect of the inclination angle is negligible for an aspect ratio of AR = 0.7.
- The convection heat transfer performance is ameliorated with the addition of composite nanoparticles. This effect is proportional to the increase of Rayleigh and Darcy numbers, the aspect ratios and the fraction of Ag in the volumetric fraction of nanoparticles.

Author Contributions: Formal analysis, M.D.M.; Funding acquisition, M.A.A.; Investigation, M.B.B.H.; Methodology, H.A.M.; Project administration, M.A.A.; Resources, M.A.A.; Software, M.B.B.H. and M.D.M.; Supervision, M.B.B.H. and H.A.M.; Validation, M.B.B.H.; Writing—original draft, M.D.M. and M.B.B.H.; Writing—review & editing, H.A.M. All authors have read and agreed to the published version of the manuscript.

Funding: This research received no external funding.

Acknowledgments: The authors would like to acknowledge the support provided by the Research Unit of Ionized Backgrounds and Reagents Studies (UEMIR) at the Preparatory Institute for Engineering Studies of Monastir (IPEIM)-Tunisia. The investigation presented in this paper was conducted as part of the research thesis in Physics Engineering at the Higher School of Sciences and Technology of Hammam Sousse (ESSTHS)-Tunisia supervised By Mohamed Bechir Ben Hamida.

Conflicts of Interest: The authors declare no conflicts of interest.

Nomenclature

AR	Aspect ratio, H/L
B_0	Magnetic field strength
Bf	Length of baffle
Cp	Specific heat, $(\mathrm{J\ Kg.K^{-1}})$
Da	Darcy number
Fr	Fraction of Ag in the volumetric fraction of nanoparticles
g	Gravitational acceleration, $(\mathrm{m\ s^{-2}})$
Gr	Grashof number
H	Width of corrugation of cavity (m)
Ha	Hartmann number
K	Permeability of porous medium, $\mathrm{m^2}$
k	Thermal conductivity, $\left(\mathrm{Wm^{-1}K^{-1}}\right)$
L	Length of cavity, (m)
Nu	Nusselt number
p	Fluid pressure, $\left(\mathrm{Pa = Nm^{-2}}\right)$
p*	Dimensionless pressure

Pr	Prandtl number
Q_0	Heat generation or absorption
q*	Dimensionless heat generation or absorption
Ra	Rayleigh number
T	Temperature, (K)
T*	Dimensionless temperature
u, v,	Velocity components in x, and y directions
u*, v*	Dimensionless velocity components
x, y,	Cartesian coordinates
x*, y*	Dimensionless coordinates
Greek symbols	
α	Thermal diffusivity m^2s^{-1}
σ	Electrical conductivity, Am V^{-1}
φ_1	Solid volume fraction of Ag nanoparticles
φ_2	Solid volume fraction of Al_2O_3 nanoparticles
β	Expansion coefficient, K^{-1}
ρ	Local density, kg m^{-3}
ΔT	Temperature difference, $T_h - T_c$, K
μ	Dynamic viscosity, kg $m^{-1}s^{-1}$
ν	Cinematic viscosity, m^2s^{-1}
ω	Angle of inclination
Subscripts	
c	Cold wall
h	Hot wall
hnf	Hybrid nanofluid
f	Fluid
l	Local
m	Average
p	Nanoparticle

References

1. Ben Hamida, M.B.; Charrada, K. Three-dimensional numerical study of different parameters effect on the external magnetic field applied to center the arc of the horizontal mercury discharge lamp. *AIP Adv.* **2015**, *5*, 107212. [CrossRef]
2. Stevanovi, P.; Cvetinovi, D.; Zivkovi, G.; Oka, S.; Pavlovi, P. Numerical modeling of disperse material evaporation in axisymmetric thermal plasma reactor. *Therm. Sci.* **2003**, *7*, 63–99. [CrossRef]
3. Ben Hamida, M.B.; Charrada, K. Contrasting the effect of electric current between the vertical and horizontal mercury discharge. *IEEE Trans. Plasma Sci.* **2013**, *41*, 7. [CrossRef]
4. Ben Hamida, M.B.; Charrada, K. Contrast the effect of the mass of mercury between the vertical and horizontal mercury discharge lamps. *IEEE Trans. Plasma Sci.* **2012**, *40*, 2065. [CrossRef]
5. Ben Hamida, M.B.; Hadj Salah, S.; Charrada, K. Total pressure and atomic ratio on transport coefficients of HgTlI discharge plasma using a LTE chemical model. *Eur. Phys. J. D* **2015**, *69*, 1–10. [CrossRef]
6. Araoud, Z.; Ben Ahmed, R.; Ben Hamida, M.B.; Franke, S.; Stambouli, M.; Charrada, K.; Zissis, G. A two-dimensional modeling of the warm-up phase of a high-pressure mercury discharge. *Phys. Plasmas* **2010**, *17*, 063505. [CrossRef]
7. Ben Hamida, M.B.; Charrada, K. Application of a three-dimensional model for a study of the energy transfer of a high-pressure mercury horizontal lamp, American Institute of Physics. *Phys. Plasmas* **2012**, *19*, 063504. [CrossRef]
8. Ben Hamida, M.B.; Helali, H.; Araoud, Z.; Charrada, K. Contrast between the vertical and horizontal mercury discharge lamps, American Institute of Physics. *Phys. Plasmas* **2011**, *18*, 063506. [CrossRef]
9. Ben Hamida, M.B.; Charrada, K. Three-dimensional dynamic study of a metal halide thallium iodine discharge plasma powered by a sinusoidal and square signal. *Eur. Phys. J. D* **2016**, *70*, 7. [CrossRef]

10. Ferjani, B.; Ben Hamida, M.B. Thermal study of the atomic ratio effect on a cylindrical and an ellipsoidal shaped HgTlI discharge lamps. *Eur. Phys. J. D* **2019**, *73*, 208. [CrossRef]
11. Ben Hamida, M.B.; Charrada, K. A three-dimensional thermal study of a mercury discharge lamp with double envelope for different orientations. *J. Plasma Phys.* **2014**, *81*, 905810202. [CrossRef]
12. Pop, I.; Ingham, D. *Convective Heat Transfer: Mathematical and Computational Modeling of Viscous Fluids and Porous Media*; Pergamon: Oxford, UK, 2001.
13. Bejan, A.; Dincer, I.; Lorente, S.; Miguel, A.; Reis, A. *Porous and Complex Flow Structures in Modern Technologies*; Springer: New York, NY, USA, 2004; p. 396.
14. Vafai, K. *Porous Media: Applications in Biological Systems and Biotechnology*; CRC Press: New York, NY, USA, 2010; p. 632.
15. Sankar, M.; Kiran, S.; Ramesh, G.; Makinde, O. Natural convection in a non-uniformly heated vertical annular cavity. *Defect Diffus. Forum.* **2017**, *377*, 189–199. [CrossRef]
16. Ben Hamida, M.B.; Massoudi, M.D.; Marzouki, R.; Kolsi, L.; Almeshaal, M.; Hussein, A.K. Study of heat and mass transfer control inside channel partially filled with a porous medium using nanofluids. *Therm. Sci.* **2019**, 460. [CrossRef]
17. Chamkha, A.J.; Selimefendigil, F. MHD free convection and entropy generation in a corrugated cavity filled with a porous medium saturated with nanofluids. *Entropy* **2018**, *20*, 846. [CrossRef]
18. Shao, Q.; Fahs, M.; Younes, A.; Makradi, A. A high-accurate solution for Darcy-Brinkman double-diffusive convection in saturated porous media. *Numer. Heat Transf. Part B Fundam.* **2016**, *69*, 26–47. [CrossRef]
19. Mohammed, H.A.; Bhaskaran, G.; Shuaib, N.H.; Saidur, R. Heat transfer and fluid flow characteristics in microchannels heat exchanger using nanofluids: A review. *Renew. Sustain. Energy Rev.* **2011**, *15*, 1502–1512. [CrossRef]
20. Mohammed, H.A.; Gunnasegaran, P.; Shuaib, N.H. Numerical simulation of heat transfer enhancement in wavy microchannel heat sink. *Int. Commun. Heat Mass Transf.* **2011**, *38*, 63–68. [CrossRef]
21. Ramanathan, A.; Gunasekaran, P. Simulation of absorption refrigeration system for automobile application. *Therm. Sci.* **2008**, *12*, 5–13. [CrossRef]
22. Ben Hamida, M.B.; Belghaeib, J.; Hajji, N. Numerical study of heat and mass transfer enhancement for bubble absorption process of ammonia water mixture without and with nanofluid. *Therm. Sci.* **2018**, *22*, 3107–3120.
23. Ben Hamida, M.B.; Belghaeib, J.; Hajji, N. Heat and mass transfer enhancement for falling film absorption process in vertical plate absorber by adding copper nanoparticles. *Arab. J. Sci. Eng.* **2018**, *43*, 4991–5001. [CrossRef]
24. Ben Jaballah, R.; Ben Hamida, M.B.; Saleh, J.; Almeshaal, M.A. Enhancement of the performance of bubble absorber using hybrid nanofluid as a cooled absorption system. *Int. J. Numer. Methods Heat Fluid Flow* **2019**, *29*, 3857–3871. [CrossRef]
25. Benhmidene, A.; Chaouachi, B.; Gabsi, S. Effect of operating conditions on the performance of the bubble pump of absorption-diffusion refrigeration cycles. *Therm. Sci.* **2011**, *15*, 793–806. [CrossRef]
26. Abdollahi, A.; Rajnish, N.; Sharma, R.N.; Mohammed, H.A.; Vatani, A. Heat transfer and flow analysis of Al_2O_3-water nanofluids in interrupted microchannel heat sink with ellipse and diamond ribs in the transverse microchambers. *Heat Transf. Eng.* **2018**, *39*, 1461–1469. [CrossRef]
27. Sheikholeslami, M.; Bandpy, M.G.; Ellahi, R.; Zeeshan, A. Simulation of MHD CuO–water nanofluid flow and convective heat transfer considering Lorentz forces. *J. Magn. Magn. Mater.* **2014**, *369*, 69–80. [CrossRef]
28. Ma, Y.; Mothibi, R.; Rashidi, M.M.; Yang, Z.; Sheremet, A.M. Numerical study of MHD nanofluid natural convection in a baffled U-shaped enclosure. *Int. J. Heat Mass Transf.* **2019**, *130*, 123–134. [CrossRef]
29. Hosseinizadeh, S.F.; Sourtiji, E. Heat transfer augmentation of magnetohydrodynamics natural convection in L-shaped cavities utilizing nanofluids. *Therm. Sci.* **2012**, *16*, 489–501.
30. Abedini, A.; Armaghani, T.; Chamkha, A.J. MHD free convection heat transfer of a water–Fe3O4 nanofluid in a baffled C-shaped enclosure. *J. Therm. Anal. Calorim.* **2019**, *135*, 685–695. [CrossRef]
31. Hussein, A.K.; Bakier, M.A.Y.; Ben Hamida, M.B.; Sivasankaran, S. Magneto-hydrodynamic natural convection in an inclined T-shaped enclosure for different nanofluids and subjected to a uniform heat source. *Alex. Eng. J.* **2016**, *55*, 2157–2169. [CrossRef]
32. Armaghani, T.; Kasaeipoor, A.; Izadi, M.; Pop, I. MHD natural convection and entropy analysis of a nanofluid inside T-shaped baffled Enclosure. *Int. J. Numer. Methods Heat Fluid Flow* **2018**, *28*, 2916–2941. [CrossRef]

33. Ahmed, M.; Shuaib, N.; Yusoff, M.; Al-Falahi, A. Numerical investigations of flow and heat transfer enhancement in a corrugated channel using nanofluid. *Int. Commun. Heat Mass Transf.* **2011**, *38*, 1368–1375. [CrossRef]
34. Hasan, M.N.; Saha, S.C.; Gu, Y. Unsteady natural convection within a differentially heated enclosure of sinusoidal corrugated side walls. *Int. J. Heat Mass Transf.* **2012**, *55*, 5696–5708. [CrossRef]
35. Hussain, S.H.; Hussein, A.K.; Mohammed, R.N. Studying the effects of a longitudinal magnetic field and discrete isoflux heat source size on natural convection inside a tilted sinusoidal corrugated enclosure. Comput. *Math. Appl.* **2012**, *64*, 476–488. [CrossRef]
36. Almeshaal, M.A.; Kalidasan, K.; Askri, F.; Velkennedy, R.; Alsagri, A.S.; Kolsi, L. Three-dimensional analysis on natural convection inside a T-shaped cavity with water-based CNT–aluminum oxide hybrid nanofluid. *J. Therm. Anal. Calorim.* **2019**, *139*, 2089–2098. [CrossRef]
37. Brinkman, H.C. The Viscosity of concentrated suspensions and solution. *J. Chem. Phys.* **1952**, *20*, 571–581. [CrossRef]
38. Maxwell, J.A. *Treatise on Electricity and Magnetism*, 2nd ed.; Oxford University Press: Cambridge, UK, 1904.
39. Ben Hamida, M.B.; Charrada, K. Natural convection heat transfer in an enclosure filled with an Ethylene Glycol-Copper nanofluid under magnetic fields. *Numer. Heat Transf. Part A Appl.* **2014**, *67*, 902–920. [CrossRef]